Journal of Science: Advanced Materials and Devices 7 (2022) 100443

Contents lists available at ScienceDirect

Journal of Science: Advanced Materials and Devices

journal homepage: www.elsevier.com/locate/jsamd

Original Article

Coordination of H_2O_2 on praseodymia nanorods and its application in sensing cholesterol

Lei Jiang [a, *], Junjie Zhong [a], Youxun Li [b], Hanyun Liu [c], Shuyuan Zhang [a], Xiudong Zhu [a], Zhibin Liu [a], Yuxue Chen [a], Susana Fernandez-Garcia [d], Xiaowei Chen [d, **]

[a] Center for Bioengineering and Biotechnology, College of Chemical Engineering, China University of Petroleum (East China), Qingdao 266580, China
[b] Marine Science Research Institute of Shandong Province & National Oceanographic Center, 7 Youyun Road, Qingdao 266104, China
[c] Department of Infectious Diseases, The Affiliated Hospital of Qingdao University, Qingdao, Shandong 266003, PR China
[d] Departamento de Ciencia de los Materiales, Ingeniería Metalúrgica y Química Inorgánica, Facultad de Ciencias and Instituto Universitario de Investigación en Microscopía Electrónica y Materiales (IMEYMAT), Universidad de Cádiz, Puerto Real, Cádiz E-11510, Spain

ARTICLE INFO

Article history:
Received 4 January 2022
Received in revised form
6 March 2022
Accepted 8 March 2022
Available online 22 March 2022

Keywords:
Praseodymium oxide
Pr_6O_{11}
Biosensing
Cholesterol
Fluorescence detection

ABSTRACT

The advancement of functional nanomaterials has promoted the development of biomarker sensors underpinning promising analytical tools for a range of bioanalytes such as cholesterol. In this work, we established a light-on fluorescent probe for cholesterol in human serum by coordination of H_2O_2 on the surface of praseodymia nanorods (Pr_6O_{11} NRs). The distinctive interactions of various nucleotides and H_2O_2 with praseodymia were examined, whereby good fluorescent quenching and recovery capability were observed. A highly sensitive and selective cholesterol detection was achieved in serum samples with a detection limit of 0.1 μM and recovery of 97.2−101.3%, respectively, due to the high oxygen mobility of praseodymia. The result suggests strong potential for work towards a key probe for a portable clinical test system for cholesterol as well as other H_2O_2-deriving biomarkers, potentially addressing the ever-increasing demand for the prevention of cardiovascular disease.

1. Introduction

Cardiovascular disease is the number one cause of death. There are approximately 17.9 million associated deaths each year, representing 32% of all global death [1]. To prevent this disease, it is important to periodically monitor cardiovascular risk markers such as plasma cholesterol. For example, based on the diagnosis and assessment of arteriosclerosis, lipid-related disorders, thrombosis, *etc* [2,3], cholesterol has to be critically controlled within suitable concentration ranges. High levels of cholesterol in serum (>6 mM) could form plaques in blood vessels, leading to atherosclerosis, cardiovascular and other diseases [2,4], while low levels of cholesterol (<3 mM) could lead to pernicious anemia, hyperthyroidism and acute infection [2,4].

To date, a variety of methods for cholesterol analysis have been developed, mainly based on monitoring the consumption of O_2 or increase of H_2O_2, which is the key byproduct of cholesterol enzymatic reactions. The measurement methods can be categorized into colorimetric [5], chromatographic [6], electrochemical [7] and fluorometric techniques [8]. Conventional colorimetric and electrochemical methods in clinical practice suffer from low sensitivity, selectivity or inconvenience, while chromatography techniques require costly and bulky equipment. In contrast, point-of-care fluorescence tests have attracted increasing interests in recent years due to their high sensitivity and the demonstrated potential of advanced portable fluorometers and smartphone-based devices [9,10]. For instance, QuantiFluor™ (Peomega Corp.) [10] have enabled on-spot measurements in outdoor environments and several smartphones integrated with analytical components have demonstrated capability in fluorescence-sensing [4,11]. The development of these cost-effective and handheld devices has suggested that on-site fluorescent analysis has great promises for a range of bioanalytes, including cholesterol detection.

Despite the advancement of fluorometers, suitable fluorescent probes or platform materials remain key challenges in this field. In *in vitro* practice, an off-on fluorescence change is much easier to detect than an on-off switch due to reduced interference from

* Corresponding author.
** Corresponding author.
E-mail addresses: leijiang@upc.edu.cn (L. Jiang), xiaowei.chen@uca.es (X. Chen).
Peer review under responsibility of Vietnam National University, Hanoi.

https://doi.org/10.1016/j.jsamd.2022.100443

surroundings. One of the main "light-on" schemes involves the construction of a sensing platform with a fluorescent probe and a quencher [10]. Herein we propose a fluorometric assay employing praseodymia nanorods (Pr_6O_{11} NRs) and fluorescently labelled DNA, which is a common fluorescent probe [10]. Both DNA and Pr_6O_{11} are abundant in nature and also available commercially. However, the fluorescence quenching capability of Pr_6O_{11} has not been fully explored. This cost-effective pair probe could be used to measure the cholesterol level in human serum with high sensitivity and selectivity, further offering potential for wider *in vitro* pathological and physiological applications.

The novelty of this assay lies in the competition between DNA nucleotides and H_2O_2 on their coordinations at surfaces of Pr_6O_{11} NRs. Pr_6O_{11} is an underexplored rare earth oxide with abundant existence in nature. This oxide has excellent chemical and physical features compared to other well-known analogues such as ceria (CeO_2), which has been commonly used as a fluorescent quencher [10,12]. Praseodymia includes a series of oxides, allowing rapid changes in oxidation state due to a variety of stable phases. One of the most stable oxides is Pr_6O_{11}, which exhibits relatively high electrical conductivity (0.954 S/cm) [13] and dielectric constant (k~ 25–30) [14] as compared with other oxidation states. This is because it has the highest intrinsic oxygen mobility among lanthanide oxides [15]. All these characteristics may contribute to fluorescence quenching and recovery [13,16,17]. By tuning DNA types and lengths, the quenching process can be optimized. The subsequent H_2O_2 coordination may cause depletion of DNA, hence inducing fluorescent "light-on". To the best of our knowledge, this is the first time such competition of coordination was reported on the surface of Pr_6O_{11} NRs. We aim to establish a highly sensitive detection of plasma cholesterol which can be demonstrated by tests using clinical samples.

2. Experimental

2.1. Synthesis of Pr_6O_{11} NRs

A hydrothermal method was used to synthesize Pr_6O_{11} NRs. A total volume of 240 mL of 6 M NaOH (Alfa Aesar, 98%) and 0.05 M $Pr(NO_3)_3 \cdot 6H_2O$ (Aldrich, 99.9%) was stirred in Teflon container for 30 min. The container was sealed and kept in 180 °C stainless steel autoclave for 24 h. Subsequently, the mixture was cooled to room temperature, centrifuged, and washed with deionized water several times, followed by ethanol wash (Panreac, Absolute Ethanol). Finally, sample was dried at 80 °C for 24 h in an oven and calcined at 500 °C for 4 h in a muffle furnace. Commercial CeO_2 nanoparticles (CeO_2 NP, 5–25 nm, 30 m^2/g, Sigma–Aldrich) were used to compare the fluorescence quenching ability with that of Pr_6O_{11} NRs.

2.2. Physical and compositional characterization

X-Ray diffraction (XRD) patterns were obtained by using a diffractometer (Empyrean, Panaco, Netherlands) with Cu Kα radiation and angle range of 20–70°. Brunauer–Emmett–Teller (BET) surface area was measured by using N_2 physisorption (Micromeritics, ASAP2020-M). Surface chemical composition and oxidation states of samples were characterized by X-ray photoelectron spectroscopy (XPS, ESCALAB 250Xi, Thermo, US). XPS spectra were recorded using monochromatized Al Ka X-Ray (1486.6 eV), with 150 W power. The spectrometer was operated in a constant analyzer energy mode, with pass energy of 30 eV. The binding energy scale was calibrated with respect to C 1s signal at 284.6 eV. After incubating Pr_6O_{11} NRs with H_2O_2 solution, NRs were washed with deionized water, dried in N_2 flow, and processed similarly for XPS measurement.

The morphology and structure of Pr_6O_{11} NRs samples were characterized using transmission electron microscope (TEM, JEM-2100UHR, Japan Electronics) with element mapping analysis. Steady state fluorescence of carboxyfluorescein (FAM) - labelled nucleotide oligomers (Sangon Biotech, Shanghai), including A_5, A_{15}, A_{30}, A_{45}, T_5, C_5, G_5, were measured by FluoroMax-4 (Horiba Jobin Yvon, France) at 485 nm excitation and 516 nm emission wavelength, respectively. The time resolved fluorescence spectroscopy was carried out in a picosecond time correlated singe photon counting (TCSPC) spectrometer (FS5, Edinburgh Instruments, UK). Zeta potential analysis of Pr_6O_{11} NRs suspension was measured by a particle size analyzer (Nano S, Malvern UK). The Fourier transform infrared (FTIR, Nicolet 6700, Thermo US) spectra of Pr_6O_{11} NRs were examined before and after incubation with H_2O_2, respectively.

All the other chemicals, including citrate, phosphate buffer solution (PBS), 4-(2-hydroxyethyl)-piperazine-1-ethanesulfonic acid (HEPES) and acetate buffer, various amino acids, and H_2O_2, were purchased from Sigma–Aldrich.

2.3. Detection of H_2O_2

FAM-A_5 oligomer (6 nM) and Pr_6O_{11} NRs (16 μg/mL) were mixed in 10 mM HEPES buffer (pH 7.6 with 150 mM NaCl) solution and incubated at room temperature for 1 h. The fluorescence change of solution was measured before and after the mixing process. Subsequently, H_2O_2 was added to deplete DNA from the DNA/Pr_6O_{11} conjugate and the fluorescence recovery was measured.

2.4. Detection of cholesterol

Cholesterol was incubated with 5 mg/mL cholesterol oxidase (ChOx) in 10 mM HEPES buffer (pH 7.6 with 150 mM NaCl) solution in darkness at 37 °C for 1 h. 20 μL incubation solution was added to 720 μL premixed FAM-A_5/Pr_6O_{11} NRs mixture that was described above. Fluorescence intensity of solution was measured again after 1 h incubation. Various molecules at 20 μM, including cysteine, lysine, histidine, serine, glutamic acid, glucose and dopamine, were added with a view to investigating effects of interferents respectively. Fluorescence changes before and after additions of interferents were compared with that of cholesterol.

2.5. Cholesterol measurement in human serum

Human serum samples were provided by the Affiliated Hospital of Qingdao University (Qingdao, China). Predetermined amounts of cholesterol were added to the serum to form spiked samples with low to high levels of cholesterol [18]. The spiked samples were incubated with 8.9 mM KOH in ethanol at 37 °C for 1 h to hydrolyze cholesterol esters. Subsequently, water and n-hexane were added and centrifuged together at 5000 rpm for 5 min followed by collection of supernatant which was subsequently evaporated in N_2 flow. The dried pellet was re-dissolved in 500-fold dilution and suspended in a solution of 1% isopropanol and 0.8% Triton X-100. 10 μL mixture of cholesterol was then incubated with 10 μL 5 mg/mL ChOx in darkness for 1 h, followed by addition of FAM-A_5/Pr_6O_{11} NRs. After fluorescent measurements, the calculated concentrations of tested samples were compared with results obtained by an automatic analyzer (Hitachi 7600, Japan), which is one of the routine analyses for cholesterol level in hospital practice.

3. Results and discussion

3.1. Synthesis and characterization of Pr_6O_{11} NRs

Pr_6O_{11} NRs were obtained using a hydrothermal synthesis method. Their morphology and structure were analyzed by TEM and XRD. Fig. 1a shows that Pr_6O_{11} NRs are uniformly shaped, with approximately 400 nm in length and 20 nm in diameter. Fig. 1b and c show the distribution of Pr and O elements of the synthesized samples, respectively. Well defined XRD peaks at (111), (200), *etc.*, are observed in Fig. 1d, aligning with those for face-centered cubic structure of Pr_6O_{11} crystals with *Fm3m* space group (JCPDS 42−1121). These peaks also indicate that the NRs have good crystalline properties with negligible impurities.

The specific surface area of Pr_6O_{11} NRs was calculated to be 27 m^2/g based on N_2 physisorption BET measurement. Pr 3d and O 1s XPS profiles are shown in Fig. 2, which were calibrated by using C 1s peak at 284.6 eV as reference (Fig. S1 in supporting information). Pr 3d peaks at 933.2 eV and 953.6 eV are associated with Pr $3d_{3/2}$ and Pr $3d_{5/2}$ components respectively [19,20]. The profile can be deconvoluted into several peaks, including two spin−orbit doublets at 928.4/949.4 eV and 933.2/953.6 eV [19,20]. These doublets are attributable to both Pr_2O_3 and Pr_6O_{11} oxides, but not to PrO_2 stoichiometric formula. Doublet at 946.6/966.1 eV corresponds to Pr^{4+} in Pr_6O_{11} [19,20]. From XPS analysis, it is estimated that Pr_6O_{11} NRs possess approximately 32% Pr^{3+}, in line with the bulk percentage 33% (based on Pr_6O_{11} formula).

The O 1s spectra in Fig. 2b are fitted with two peaks at 528.6 eV and 531.4 eV. The peak at 528.6 eV is for O^{2-} in the bulk, or oxygen of Pr−O bonds in the lattice. The 531.4 eV peak corresponds to surface oxygen ions, defect oxides, or adsorbed oxygen species [19]. After the subpeak fitting, the relative quantity of surface oxygen can be estimated. It was estimated that approximately 28% of oxygen was lattice oxygen while surface oxygen dominated with 72% of the total oxygen. We also examined the XPS profiles of Pr_6O_{11} NRs after incubating with H_2O_2 in order to explore the modification that H_2O_2 may impose on Pr_6O_{11} surfaces. Composition analysis showed that surface oxygen increased to 83% after incubating with H_2O_2. It is inferred that H_2O_2 forms peroxo complex Pr−H_2O_2 on Pr_6O_{11} NRs surface, leading to the increase of surface oxygen.

3.2. Fluorescent "light-off" on Pr_6O_{11} NRs

Fig. 3 displays the fluorescence "off-on" mechanism for cholesterol measurement on the surface of Pr_6O_{11} NRs. First, fluorescence of FAM-labelled oligomers was quenched ("light-off") due to adsorption and coordination of nucleotides to Pr_6O_{11} surface. Next, cholesterol-derived H_2O_2 quickly adsorb, compete and replace oligomers so that fluorescence on the depleted oligomers was recovered ("light-on"). Finally, the quantitative dependence of H_2O_2 and cholesterol concentration on fluorescence was established, which was further employed for testing of clinical samples.

Fig. 4a shows the fluorescence change at 516 nm of FAM-A_5 before and after addition of Pr_6O_{11} NRs. Fluorescence intensity

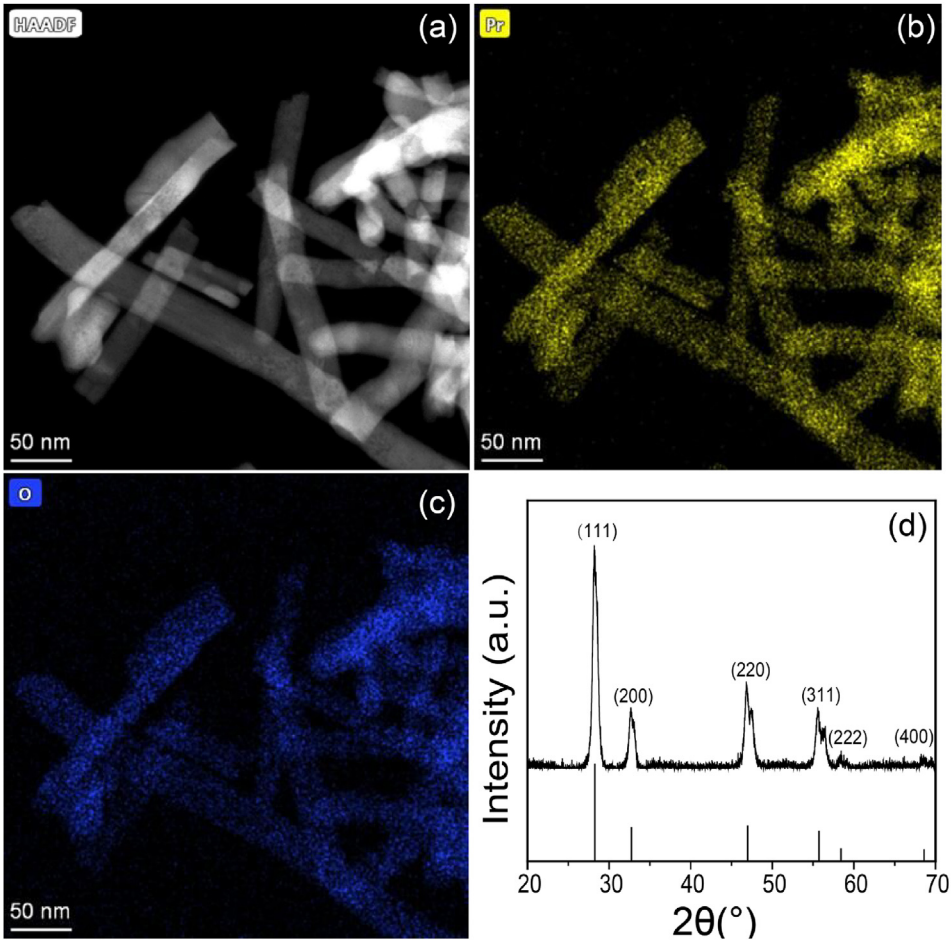

Fig. 1. (a) STEM-HAADF image, (b) Pr (c) O element mapping analysis, and (d) XRD pattern of Pr_6O_{11} NRs.

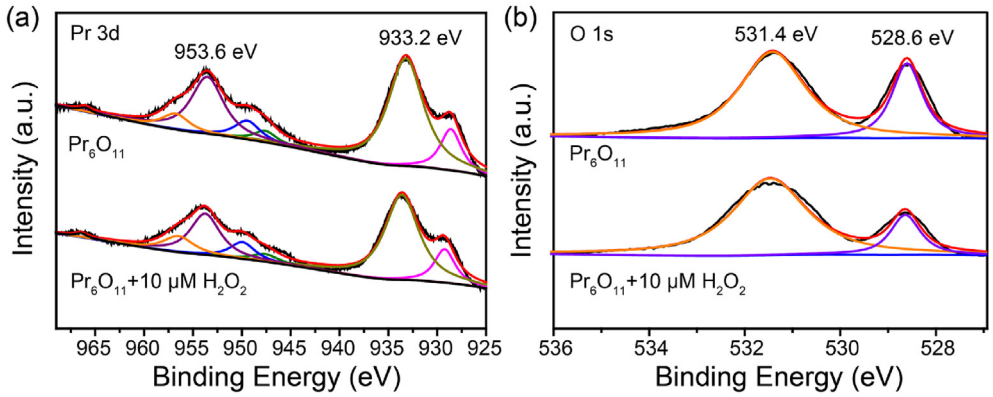

Fig. 2. (a) Pr 3d and (b) O 1s XPS spectra of Pr_6O_{11} NRs, before and after mixing with 10 μM H_2O_2.

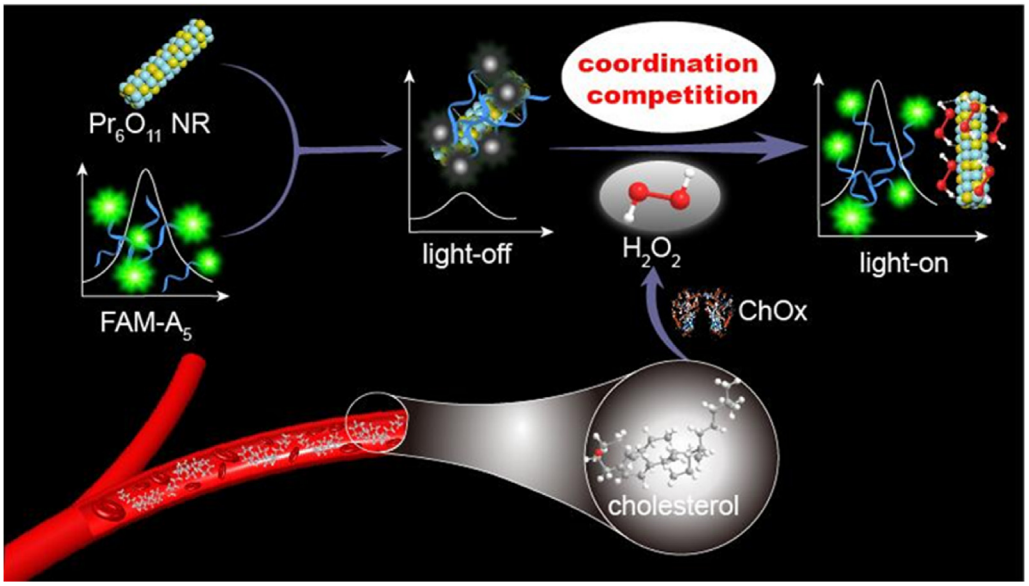

Fig. 3. Fluorescence "off-on" mechanism for highly sensitive detection of cholesterol through the competition between FAM-A_5 oligomers and H_2O_2 on their coordination at surfaces of Pr_6O_{11} NRs.

drops significantly with successive addition of Pr_6O_{11} NRs, up to 95%. The intensity decrease is proportional to concentration of Pr_6O_{11} NRs. Fig. 4b indicates that majority of the quenching occurred within 2 min from after the addition of NRs. The attraction of DNA toward Pr_6O_{11} NRs is expected as Pr_6O_{11} can be regarded as hard Lewis acid while DNA behaves like a hard base according to hard soft base theory (HSAB) [21]. Additionally, three factors may contribute to adsorption and quenching of DNA. First, there is an electrostatic attraction between negative DNA and positive Pr_6O_{11} surface (20 mV zeta potential in pH 7 buffer). Second, there is an entropy gain when the immobilized DNA leads to the release of numerous counterions that were previously bound in double layers near charged Pr_6O_{11} surfaces. Third, there may be coordination bonds between Pr and nucleotide bases, which will be discussed in section 3.3. The combination of these possible causes could be responsible for the fast adsorption and quenching of fluorescent DNA oligomers.

As shown in Fig. 4c, quenching could take place via two possible mechanisms, *i.e.* energy or electron transfer. Energy transfer usually occurs through fluorescence resonance energy transfer (FRET) effect [21]. For example, Pr_6O_{11} has a wide absorption band in 400–700 nm spectrum range (Fig. S2), corresponding to *f*–*f* transition absorption and to the characteristic transition of Pr^{3+} $^3P_0 \rightarrow {}^3H_4$. It covers the emission spectra of FAM (516 nm), suggesting that energy could transfer from the excited FAM* to Pr_6O_{11}. Alternatively, because of high conductivity of Pr_6O_{11}, quenching can happen through electron transfer from FAM* to conduction band (CB) of Pr_6O_{11} (Fig. 4c). Furthermore we found that, at the same conditions, quenching efficiency of Pr_6O_{11} NRs is much better than its neighbor compound CeO_2, which is a commonly used quenching nanomaterial (Fig. S3a) [10,12]. The defect-rich CeO_2 nanoparticles (various-shaped nanocrystals, BET 30 m^2/g, size 5–25 nm, TEM image in Fig. S3b) were expected to quench more effectively than Pr_6O_{11} NRs (uniform-shaped, 27 m^2/g, size 400 × 20 nm). However, Fig. S3a shows the opposite result, suggesting that intrinsically Pr_6O_{11} may have higher capability in transfering energy or electron than CeO_2.

The time resolved fluorescence spectroscopy provides kinetics of fluorescence quenching, which can be briefly classified into static and dynamic modes [22]. Static mode occurs when a ground state complex between fluorophore and quencher is formed, while dynamic mode is often due to diffusion of quencher to fluorophore

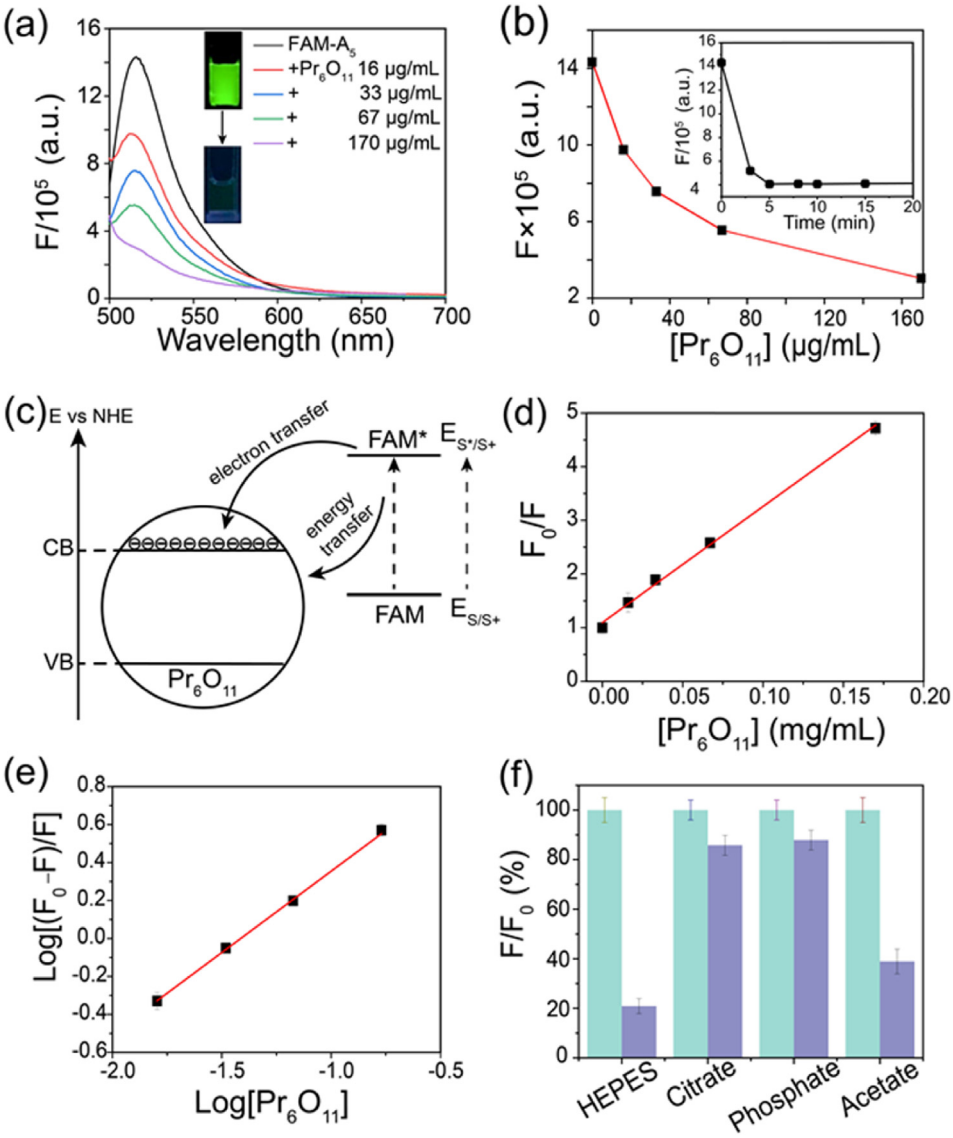

Fig. 4. (a) Fluorescence spectra of 6 nM FAM-A_5 with Pr_6O_{11} NRs in pH 7.6 HEPES buffer. Inset images show "light-off" of fluorescence. (b) Fluorescence at 516 nm changes with time after adding 67 μg/mL Pr_6O_{11} NRs to FAM-A_5. Inset is the relationship between fluorescence intensity and Pr_6O_{11} NRs concentration. (c) Energy level diagram of Pr_6O_{11} shows how fluorescence quenching occurs through energy or electron transfer, from excited FAM* dye to Pr_6O_{11}. (d) Plot of intensity ratio F_0/F of FAM-A_5 against Pr_6O_{11} NRs concentration, fitted by the classical Stern–Volmer equation (red line). (e) Plot of $log[(F_0–F)/F]$ against Pr_6O_{11} NRs concentration, fitted by the Hill equation (red line). (f) Effect of buffer type on fluorescence quenching.

when the latter is in an excited state. In order to investigate the binding state of oligomers with Pr_6O_{11} NRs, the classical Stern–Volmer equation (Eq. (1)) is used to fit data where F_0 and F are fluorescence intensities before and after addition of quenchers [23,24]. In Eq. (1), C_{Pr6O11} is the concentration of Pr_6O_{11} NRs, τ_0 the average lifetime of biomolecules without quencher (~10^{-8} s), K_q the quenching rate constant and K_{SV} the Stern–Volmer quenching coefficient.

$$F_0/F = K_{SV}\, C_{Pr6O11} + 1 = K_q\, \tau_0\, C_{Pr6O11} + 1 \quad (1)$$

Fig. 4d shows the linear fitting of Pr_6O_{11} quenching using Eq. (1), whereby K_q is calculated to be 6.22×10^{12} $M^{-1}s^{-1}$. As reported previously [23,24], the maximum scattering collisional quenching coefficient for K_{diffu} biomolecules is 2×10^{10} $M^{-1}s^{-1}$, where $K_q >> K_{diffu}$ means that Pr_6O_{11}-induced quenching was dominated by static mode [23]. This suggests that FAM-A_5 oligomers have formed strong conjugation with Pr_6O_{11} NRs. Moreover, the number of binding site n can be calculated based on Eq. (2), *i.e.* the Hill Equation, where the equilibrium association constant K_a is the ratio of (FAM-A_5/Pr_6O_{11} NRs) conjugates concentration to the concentration of FAM-A_5 and Pr_6O_{11} NRs as in Eq. (3) [24].

$$\log[(F_0–F)/F] = \log K_a + n \log C_{Pr6O11} \quad (2)$$

$$K_a = C_{conjugate} / C_{FAM\text{-}A5}\, C_{Pr6O11} \quad (3)$$

Parameter n is dimensionless as a measure for cooperativity in the binding process. Fig. 4e shows a logarithmic plot of $[(F_0–F)/F]$ vs C_{Pr6O11} which was fitted to provide an estimated n ~ 1.21. This n value is greater than unity, suggesting a positive cooperativity binding [24], It means binding of an oligomer facilitates binding of the subsequent oligomers at nearby sites on Pr_6O_{11} surfaces.

Similar to the previously reported quenchers [10,12], this Pr_6O_{11}-induced quenching depends on buffer types. Quenching is more effective in HEPES buffer than in other buffers, such as citrate, phosphate and acetate buffers (Fig. 4f). This is probably because HEPES ions do not precipitate or adsorb on nanorod surface as much as other buffer ions do, like the strong attachment of phosphate ions to CeO_2 surfaces [25].

3.3. Fluorescent "light-on" through H_2O_2 coordination

When H_2O_2 was added to FAM-A_5/Pr_6O_{11} NRs mixture, the quenched fluorescence at 516 nm can be greatly recovered (Fig. 5a). The recovery level increases with H_2O_2 concentration (Fig. 5b), suggesting the release of FAM-A_5 oligomers off NRs surfaces. As shown in Fig. 5b inset, the increase is linear and proportional to H_2O_2 concentration in $\leq$10 μM range. It is worth noting that 1–10 μM range is also the physiological range of H_2O_2 in human plasma across normal and abnormal ranges [26,27], implying the potential applicability of FAM-A_5/Pr_6O_{11} NRs probe in detection of H_2O_2 and H_2O_2-generating biomarkers, such as cholesterol and glucose.

Fluorescence recovery depends on salt, nucleotide type and length. Fig. 5c shows the restored intensity as a function of NaCl concentration. Increase of salt concentration corresponds to higher recovery which reaches a maximum at 150 mM NaCl. This may be due to screening effect of salt on eliminating double layer repulsion from negative oligomer surfaces. The presence of more counterions weakens the electrostatic attraction between DNA and NRs. Thus, the released DNA, as well as recovered fluorescence, is more stable in salted conditions, until charge neutralization reaches maximum. Similarly, Fig. 5d indicates that shorter sequences perform better than longer ones. This is probably because high mobility of shorter strands facilitates faster adsorption and desorption on NRs surfaces as compared with that of longer strands.

Quenching and recovery also vary for different nucleotide bases. DNA has polymerized anionic phosphate backbones which help to

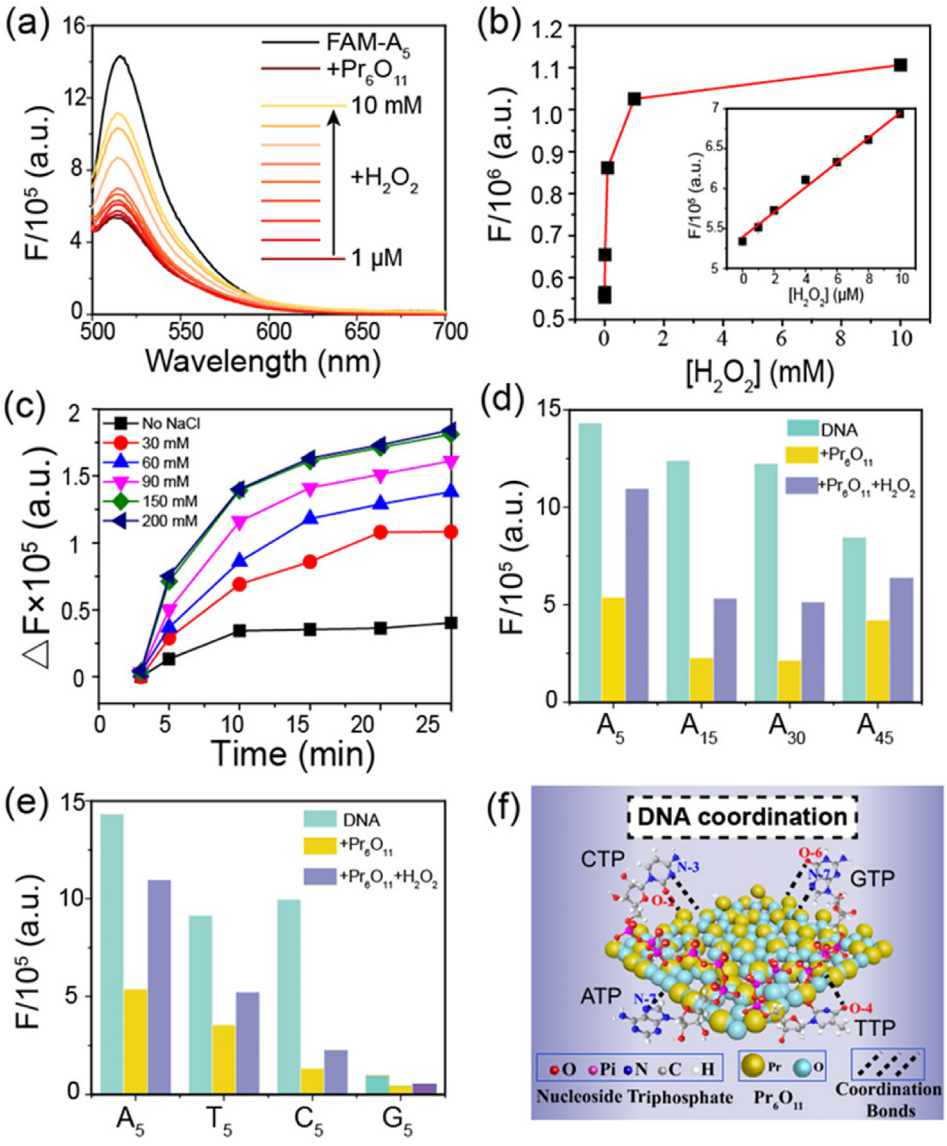

Fig. 5. (a) Fluorescence recovery of 6 nM FAM-A_5 with 67 μg/mL Pr_6O_{11} NRs after H_2O_2 addition at increasing concentration (1 μM–10 mM) in pH 7.6 HEPES buffer. (b) Relationship between fluorescence and H_2O_2 concentration. Inset is the linear fitting of fluorescence intensity with H_2O_2 at 1–10 μM. Limit of detection (LOD, s/n = 3) is 0.1 μM with $R^2 = 0.99$. (c) Effect of NaCl salt on fluorescence change with 8 μM H_2O_2. Effects of nucleotide (d) length and (e) type on fluorescence quenching and recovery are compared. (f) Possible coordination of nucleotide bases (adenine, guanine, cytosine and thymine) with Pr atoms on Pr_6O_{11} NRs surface.

promote its binding process to NRs although difference in stacked bases determines binding affinities. Fig. 5e shows that quenching and recovery are more pronounced in FAM-A_5 than in T_5 and C_5. FAM-G_5 has particularly low fluorescence because guanine itself is a quenching agent [28]. Previous studies have suggested strong chemical bondings between metals and DNA bases [28]. For instance, deoxyadenosine base prefers to coordinate with metal atoms via both N-6 exocyclic amino and N-7 atom (Fig. 5f), while deoxyguanosine binds through C=O with N-1 nitrogen [28]. Deoxycytidine binds via N-3 nitrogen as well as the keto oxygen while thymine binds through C-4 keto oxygen [28]. Variation in coordination defines orientation and binding strength of different bases to Pr_6O_{11}. This directly impacts on the total binding strength of oligomers on Pr_6O_{11} NRs, as well as their capabilities to compete with H_2O_2. Consequently, different nucleotide types result in varying fluorescence quenching and recovery with Pr_6O_{11} and H_2O_2.

The schematic process of H_2O_2 coordination and the subsequent release of DNA is illustrated in Fig. 6a. Despite differential bindings between nucleotides and Pr_6O_{11}, data suggests that H_2O_2 coordination with Pr_6O_{11} is much stronger than oligomers' coordination, even if DNA possesses forces from both electrostatic attraction and base coordination. H_2O_2 is known to be able to coordinate with many metal atoms, including Fe^{3+}, Cu^{2+}, *etc*, particularly in presence of OH^- ions [29]. In this study, under weak basic (pH 7.6) environment, it is possible that H_2O_2 was deprotonated on NRs surface to form stable peroxo complex (Fig. 6a). Similar peroxo structures have been reported for H_2O_2 coordination to many peroxidase-like nanomaterials such as Co−MoS_2 and single atom catalysts [30]. It was proposed that H_2O_2 coordination is the start of free radical chain reaction triggered by the accelerated electron transfer and formation of intermediate hydroxyl radicals. Our previous experiments have confirmed peroxidase-like activity of Pr_6O_{11} NRs (data not shown). Thus, it is likely that H_2O_2 also have strong tendency to form such peroxo structures on Pr_6O_{11} NRs.

Formation of Pr−H_2O_2 coordination complex was supported by XPS data as shown in Fig. 2. Further zeta potential (Fig. 6b) and FTIR (Fig. 6c) results also agree with the analysis that slight increase of zeta potential is probably due to H_2O_2 displacement of counterions, leading to total charges alternation on NRs surfaces. The 733 cm^{-1} peak in FTIR spectra is attributable to the vibration of Pr-O-H bonds, while the peak at 3616 cm^{-1} corresponds to stretching and vibration O−H bonds on Pr_6O_{11} NRs after H_2O_2 impregnation. Therefore, it is likely that H_2O_2 forms covalent peroxo bonds on Pr_6O_{11} surface. In other words, the chemical bondings between H_2O_2 and NRs are stronger than those between DNA and NRs, effectively leading to the removal of DNA oligomers from NRs surfaces.

DNA displacement by H_2O_2 does not seem favorable based on entropy theories. In particular, in order to fill the void space on NRs induced by the removal of a DNA oligomer requires the immobilization of many H_2O_2 molecules, thus reducing entropy. However, it is worth noting that the H_2O_2 coordination on NRs surfaces also increase total oxygen reservoir of Pr_6O_{11} NRs. Pr_6O_{11} exhibits exceptionally high oxygen mobility and thus it is plausible to assume that the enlarged oxygen reservoir gains much more entropy. As a result, the total entropy is increased on H_2O_2 coordination and hence the process is dynamically favorable.

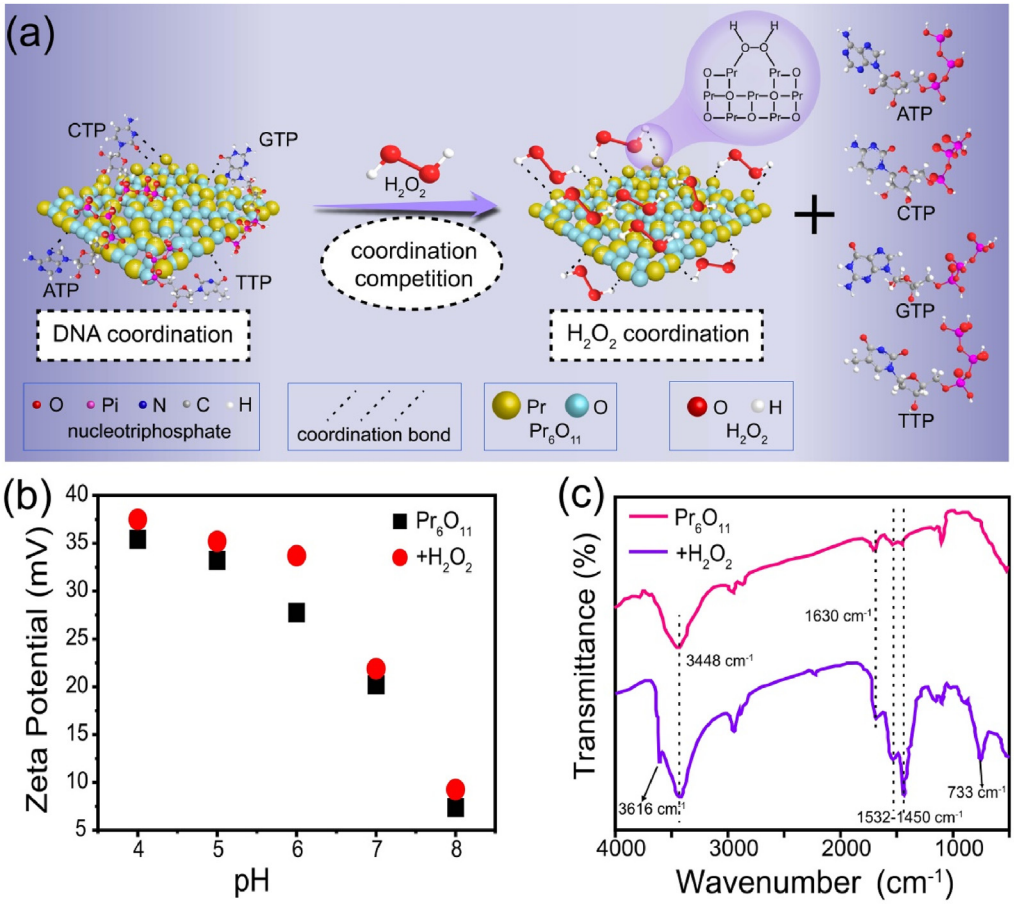

Fig. 6. (a) Competition between H_2O_2 and DNA in coordinating with Pr_6O_{11} results in release of DNA and binding of H_2O_2 on NRs surface. (b) Zeta potential changes on addition of 10 μM H_2O_2 to Pr_6O_{11} NRs suspension in HEPES buffer. (c) FTIR spectra of Pr_6O_{11} NRs before and after incubation with 10 μM H_2O_2.

3.4. Highly sensitive detection of cholesterol

A highly sensitive detection platform for H_2O_2 and cholesterol could be established, based on the mechanism depicted above, by using FAM-A_5/Pr_6O_{11} NRs pair probes (Fig. 1). Fig. 5b shows a linear relationship between fluorescence change and H_2O_2 concentration, as well as the corresponding limit of detection (LOD, s/n = 3) of 0.1 μM. This value is lower than mostly reported fluorescent "light-on" measurements of H_2O_2 (Table S1) thus far.

Fig. 7a demonstrates fluorescence recovery of FAM-A_5/Pr_6O_{11} NRs system with addition of cholesterol. The fluorescence intensity increases linearly with cholesterol concentration between 1 and 12 μM (Fig. 7b) with LOD (s/n = 3) of 0.1 μM. This represents much improved performance as compared (Fig. 7c) with other reported results whereby fluorescent probes were used for cholesterol detection, including "light-on" or "light-off" assays (Table S2).

It is worth noting that the linear ranges of various detection methods on H_2O_2 or cholesterol are not specifically discussed or compared (data shown in Table S1 and S2) because we believe LOD is probably a better metric to assess the effectiveness among cholesterol sensing and analysis systems than linear ranges. First, it was not our focus to compare H_2O_2 > 10 μM, which is beyond the physiological range. Second, it is important to note that essential pretreatment of clinical samples, including digestion and dilution of serum, could always result in suitable range of cholesterol concentration for detection. Thus, LOD may be a better indicator than linear ranges in comparison among different detection systems.

Several serum constituents including amino acids, glucose, dopamine, *etc.* were examined using our "light-on" platform with a view to identifying their possible interference. Results (Fig. 7d and Fig. S4) show that the interference is negligible as compared with that from cholesterol, suggesting excellent cholesterol sensing selectivity. Finally, a standard addition method was applied with a series of spiked cholesterol contents in human serum samples in order to evaluate the practicability of this method. Results (Table 1) indicate that our measurements are in good agreement with certified values obtained from an automatic analyzer which is one of the routine methods in hospital practice. The relative standard deviation (RSD ≤3.1%) and recovery (97.2–101.3%) are also achieved, demonstrating good consistency across our testing samples.

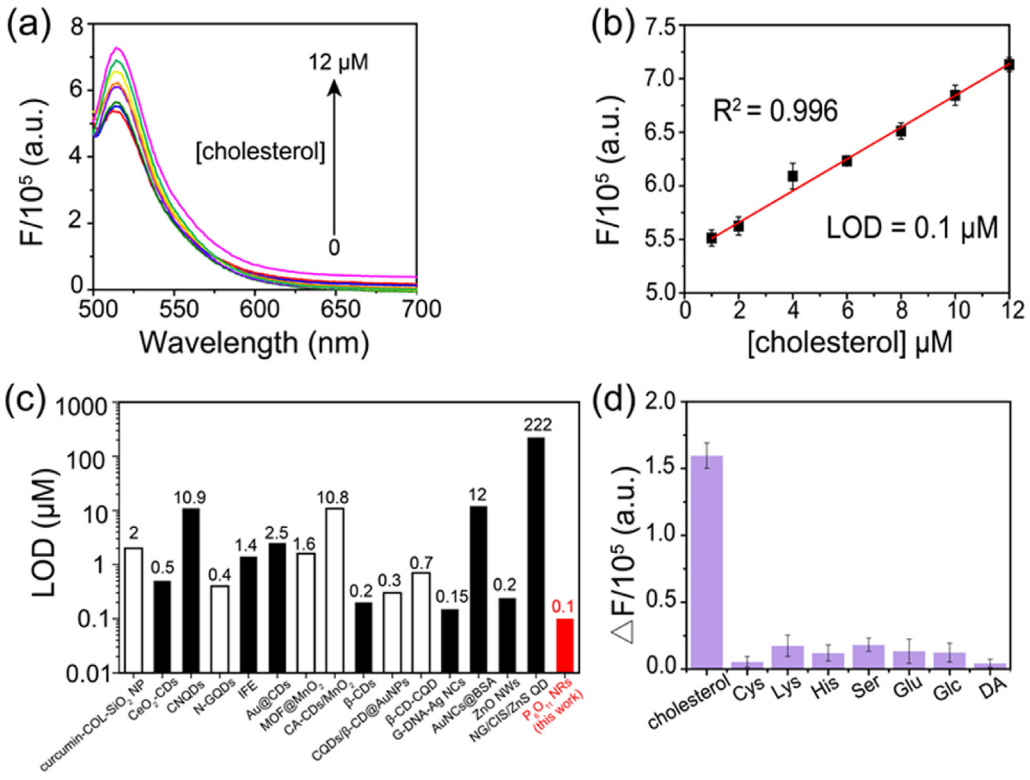

Fig. 7. (a) Fluorescence increase of 6 nM FAM-A_5 + 67 μg/mL Pr_6O_{11} NRs mixture after addition of cholesterol. (b) Relationship between fluorescence intensity and cholesterol concentration. The solid line is linear fit with R^2 = 0.996 and LOD of 0.1 μM. (c) Comparison of LODs from the latest measurements of cholesterol using "light-on" (full bars) and "light-off" (empty bars) fluorescence methods (details in Table S2 of supporting information). (d) Fluorescence from possible serum interferents, including cysteine (Cys), lysine (Lys), histidine (His), serine (Ser), glutamic acid (Glc), glucose (Glu) and dopamine (DA), are compared with that of cholesterol.

Table 1
measurements of cholesterol in clinical samples.

Samples	Added (mM)	Measured (mM)	Recovery (%)	RSD (%)	Certified Value (mM)
Serum		4.3		2.2	4.4
	2.5	6.9	98	3.1	6.9
	7.1	11.3	97.2	1.8	11.5
	7.9	12.4	101.3	2.5	12.3

4. Conclusion

A fluorescent "light-on" platform for cholesterol detection is constructed based on functional Pr_6O_{11} NRs and fluorescent DNA oligomers (FAM-A_5). Fluorescence of adsorbed DNA can be efficiently quenched due to high electron transfer and oxygen mobility of Pr_6O_{11}, while strong coordination of H_2O_2 can displace oligomers. The mechanism of coordination and fluorescent response is discussed in detail and, to the best of our knowledge, is for the first time reported for Pr_6O_{11} nanomaterial. Highly sensitive and selective detection of cholesterol is achieved, with exceptionally low LOD of 0.1 μM (s/n = 3) and good recovery demonstrated by using clinical samples. It is envisaged that this method can be potentially utilized for the detection of other H_2O_2-related biomarkers such as glucose and hypoxanthine. This platform enables *in vitro* monitoring of cholesterol, with potential applications in handheld fluorometers or smartphone-integrated devices. Using fluorometers such as QuantiFluor™ and oligomers, this method could be particularly helpful for fast clinical analysis of cholesterol in and out of hospital settings.

Declaration of competing interest

The authors declare that they have no known competing financial or personal relationships that could have appeared to influence the work reported in this paper.

Acknowledgements

This work was supported by the Natural Science Foundation of Shandong Province (Grant ZR2017LB028), Key R&D Program of Shandong Province (Grant 2018GSF118032), and Fundamental Research Funds for the Central Universities (Grant 18CX02125A) in China. The project with reference number of ENE2017-82451-C3-2-R from Ministry of Science, Innovation and Universities of Spain is also acknowledged. This work has been co-financed by the 2014–2020 ERDF Operational Programme and by the Department of Economy, Knowledge, Business and University of the Regional Government of Andalusia with reference number of FEDER-UCA18-107316.

Appendix A. Supplementary data

Supplementary data to this article can be found online at https://doi.org/10.1016/j.jsamd.2022.100443.

References

[1] World health organization (WHO). Fact Sheet. http://www.who.int/mediacentre/factsheets/fs317/en/.
[2] L. Yang, H. Zhao, S. Fan, G. Zhao, X. Ran, C.-P. Li, Electrochemical detection of cholesterol based on competitive host–guest recognition using a β-cyclodextrin/poly(N-acetylaniline)/graphene-modified electrode, RSC Adv. 5 (79) (2015) 64146–64155.
[3] X. Miao, Z. Cheng, Z. Li, P. Wang, A novel sensing platform for sensitive cholesterol detection by using positively charged gold nanoparticles, Biochem. Eng. J. 117 (2017) 21–27.
[4] X. Meng, T. Shi, Y. Lu, Fabrication of a novel β-CD-based fluorescence probe for the targeted detection of cholesterol, J. Mater. Sci. 55 (14) (2020) 6078–6092.
[5] C. Hong, X. Zhang, C. Wu, Q. Chen, H. Yang, D. Yang, Z. Huang, R. Cai, W. Tan, On-site colorimetric detection of cholesterol based on polypyrrole nanoparticles, ACS Appl. Mater. Interfaces 12 (49) (2020) 54426–54432.
[6] M. Beggio, C. Cruz-Hernandez, P.-A. Golay, L.Y. Lee, F. Giuffrida, Quantification of total cholesterol in human milk by gas chromatography, J. Separ. Sci. 41 (8) (2018) 1805–1811.
[7] B.K. Shrestha, R. Ahmad, S. Shrestha, C.H. Park, C.S. Kim, In situ synthesis of cylindrical spongy polypyrrole doped protonated graphitic carbon nitride for cholesterol sensing application, Biosens. Bioelectron. 94 (2017) 686–693.
[8] J. Li, T. Liu, S. Liu, J. Li, G. Huang, H.-H. Yang, Bifunctional magnetic nanoparticles for efficient cholesterol detection and elimination via host-guest chemistry in real samples, Biosens. Bioelectron. 120 (2018) 137–143.
[9] Y. Li, J. Cai, F. Liu, H. Yang, Y. Lin, S. Li, X. Huang, L. Lin, Construction of a turn off-on fluorescent nanosensor for cholesterol based on fluorescence resonance energy transfer and competitive host-guest recognition, Talanta 201 (2019) 82–89.
[10] G. Bulbul, A. Hayat, F. Mustafa, S. Andreescu, DNA assay based on nanoceria as fluorescence quenchers (NanoCeracQ DNA assay), Sci. Rep. 8 (2018).
[11] H. Rao, W. Liu, K. He, S. Zhao, Z. Lu, S. Zhang, M. Sun, P. Zou, X. Wang, Q. Zhao, Y. Wang, T. Liu, Smartphone-based fluorescence detection of Al^{3+} and H_2O based on the use of dual-emission biomass carbon dots, ACS Sustain. Chem. Eng. 8 (23) (2020) 8857–8867.
[12] B. Liu, Z. Sun, P.-J.J. Huang, J. Liu, Hydrogen peroxide displacing DNA from nanoceria: mechanism and detection of glucose in serum, J. Am. Chem. Soc. 137 (3) (2015) 1290–1295.
[13] M.S. Hassan, M.S. Akhtar, K.-B. Shim, O.-B. Yang, Morphological and electrochemical properties of crystalline praseodymium oxide nanorods, Nanoscale Res. Lett. 5 (4) (2010) 735–740.
[14] M. Uma, M.S.P. Reddy, K.R. Reddy, V.R. Reddy, Electrical and carrier transport properties of Au/Pr_6O_{11}/n-GaN MIS structure with a high-k rare-earth oxide interlayer at high temperature range, Vacuum 174 (2020).
[15] N.K. Chandar, R. Jayavel, Structural, morphological and optical properties of solvothermally synthesized $Pr(OH)_3$ nanoparticles and calcined Pr_6O_{11} nanorods, Mater. Res. Bull. 50 (2014) 417–420.
[16] S. Majeed, S.A. Shivashankar, Pr_6O_{11} micro-spherical nano-assemblies: microwave-assisted synthesis, characterization and optical properties, Mater. Chem. Phys. 143 (1) (2013) 155–160.
[17] S. Zinatloo-Ajabshir, M. Salavati-Niasari, Nanocrystalline Pr_6O_{11}: synthesis, characterization, optical and photocatalytic properties, New J. Chem. 39 (5) (2015) 3948–3955.
[18] P.T. Nguyen, Y.I. Kim, M.I. Kim, Reagent-free colorimetric cholesterol test strip based on self color-changing property of nanoceria, Front. Chem. 8 (2020) 798.
[19] A.G. Shende, S.G. Ghugal, D. Vidyasagar, S.B. Kokane, Jagannath, S.S. Umare, R. Sasikala, Solvent free solid-state synthesis of Pr_6O_{11}/g-C_3N_4 visible light active photocatalyst for degradation of AV7 dye, Mater. Res. Bull. 107 (2018) 154–163.
[20] B.M. Abu-Zied, Controlled synthesis of praseodymium oxide nanoparticles obtained by combustion route: effect of calcination temperature and fuel to oxidizer ratio, Appl. Surf. Sci. 471 (2019) 246–255.
[21] B. Liu, J. Liu, Sensors and biosensors based on metal oxide nanomaterials, TrAC Trends Anal. Chem. 121 (2019) 115690.
[22] J. Yu, N. Song, Y.-K. Zhang, S.-X. Zhong, A.-J. Wang, J. Chen, Green preparation of carbon dots by Jinhua bergamot for sensitive and selective fluorescent detection of Hg^{2+} and Fe^{3+}, Sensor. Actuator. B Chem. 214 (2015) 29–35.
[23] N. Nagarajan, G. Paramaguru, G. Vanitha, R. Renganathan, Photosensitization of colloidal SnO_2 semiconductor nanoparticles with Xanthene Dyes, J. Chem. 2013 (2013).
[24] S. Seyedi, P. Parvin, A. Jafargholi, S. Jelvani, M. Shahabi, M. Shahbazi, P. Mohammadimatin, A. Moafi, Fluorescence properties of Phycocyanin and Phycocyanin-human serum albumin complex, Spectrochim. Acta Mol. Biomol. Spectrosc. 239 (2020).
[25] J.T. Dahle, K. Livi, Y. Arai, Effects of pH and phosphate on CeO_2 nanoparticle dissolution, Chemosphere 119 (2015) 1365–1371.
[26] V.A. Guarino, W.M. Oldham, J. Loscalzo, Y.-Y. Zhang, Reaction rate of pyruvate and hydrogen peroxide: assessing antioxidant capacity of pyruvate under biological conditions, Sci. Rep. 9 (2019).
[27] H.J. Forman, A. Bernardo, K.J.A. Davies, What is the concentration of hydrogen peroxide in blood and plasma? Arch. Biochem. Biophys. 603 (2016) 48–53.
[28] J. Liu, Adsorption of DNA onto gold nanoparticles and graphene oxide: surface science and applications, Phys. Chem. Chem. Phys. 14 (30) (2012) 10485–10496.
[29] L.-S. Lin, T. Huang, J. Song, X.-Y. Ou, Z. Wang, H. Deng, R. Tian, Y. Liu, J.-F. Wang, Y. Liu, G. Yu, Z. Zhou, S. Wang, G. Niu, H.-H. Yang, X. Chen, Synthesis of copper peroxide nanodots for H_2O_2 self-supplying chemodynamic therapy, J. Am. Chem. Soc. 141 (25) (2019) 9937–9945.
[30] Y. Zhang, S. Ni, C. Chong, J. Xu, X. Mu, X.-D. Zhang, Biocatalysts at atom level: from coordination structure to medical applications, Appl. Mater. Today 23 (2021) 101029.